Analytica Chimica Acta 1184 (2021) 339019

Contents lists available at ScienceDirect

Analytica Chimica Acta

journal homepage: www.elsevier.com/locate/aca

Predicting ion mobility as a function of the electric field for small ions in light gases

Viraj D. Gandhi [a, b], Carlos Larriba-Andaluz [b, *]

[a] Mechanical Engineering, Purdue University, 610 Purdue Mall, West Lafayette, 47907, Indiana, United States
[b] Mechanical Engineering, Indiana University Purdue University - Indianapolis, 723 W Michigan Street, Indianapolis, 46202, Indiana, United States

HIGHLIGHTS

- Consistent ion mobility calculations as a function of the field using all-atom models in Helium gas have been attempted.
- The calculations have been performed using the first and fourth approximation to the two-temperature theory.
- The resulting numerical mobilities are within 4% (first order) and 3% (fourth order) of their experimental counterpart.
- The effects of well-depth ε and polarizability α_p were studied. The combined effect is responsible for the hump in the $K_0 - E/N$ curves.
- Inelastic collisions may be important for heavier gases but can be mostly neglected for Helium under the E/N range studied.

GRAPHICAL ABSTRACT

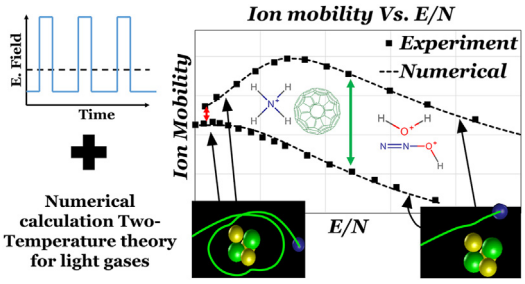

ARTICLE INFO

Article history:
Received 8 May 2021
Received in revised form
7 August 2021
Accepted 30 August 2021
Available online 6 September 2021

Keywords:
Ion mobility
High field
FAIMS
DMS
Two-temperature approximation
Mass spectrometry

ABSTRACT

High resolution mobility devices such as Field Asymmetric Waveform Ion Mobility Spectrometry (FAIMS) and Differential Mobility spectrometers (DMS) use strong electric fields to gas concentration ratios, E/N, to separate ions in the gas phase. While extremely successful, their empirical results show a non-linear, ion-dependent relation between mobility K and E/N that is difficult to characterize. The one-temperature theory Mason-Schamp equation, which is the most widely used ion mobility equation, unfortunately, cannot capture this behavior. When the two-temperature theory is used, it can be shown that the $K - E/N$ behavior can be followed quite closely numerically by equating the effect of increasing the field to an increase in the ion temperature. This is attempted here for small ions in a Helium gas environment showing good agreement over the whole field range. To improve the numerical characterization, the Lennard-Jones (L-J) potentials may be optimized. This is attempted for Carbon, Hydrogen, Oxygen and Nitrogen at different degrees of theory up to the fourth approximation, which is assumed to be exact. The optimization of L-J improves the accuracy yielding errors of about 3% on average. The fact that a constant set of L-J potentials work for the whole range of E/N and for several molecules, also suggests that inelastic collisions can be circumvented in calculations for He. The peculiar $K - E/N$ hump behaviors are

* Corresponding author.
E-mail address: clarriba@iupui.edu (C. Larriba-Andaluz).

https://doi.org/10.1016/j.aca.2021.339019

studied, and whether mobility increases or decreases with E/N is shown to derive from a competition between relative kinetic energy and the interaction potentials.

1. Introduction

The effect of the electrical field on ion mobility has become of growing importance in the field of analytical chemistry due to the use of high-field separation instruments such as Differential Mobility Spectrometers (DMS), Field Asymmetric ion mobility spectrometers (FAIMS) or even Traveling wave spectrometers (T-wave) [1–4]. However, the understanding of how mobility varies with the electric field is not well-known, especially in the case of polyatomic ions. This work portrays a complete theoretical and numerical framework that enables the calculation of mobility at high fields accurately for any ion if the proper level of theory is applied. The consequences of being able to calculate mobilities as a function of field and/or temperatures with this detail surpasses the field of analytical chemistry, and has important repercussions in non-equilibrium chemistry, gas-phase chemical kinetics, thermochemistry, combustion, plasma chemistry and physical chemistry.

Gas phase ions in the presence of an electric field accelerate and their increase in velocity is met by an increasing collisional drag force until an equilibrium drift velocity is reached [5]. Based on this drift velocity, ions can be separated by their arrival time to the detector, as ion effective size and drift velocity are inversely related [6,7]. The relationship between drift velocity v_d and electric field E yields the mobility K of the ion as defined by [8]:

$$K = \frac{v_d}{E}. \tag{1}$$

The mobility of an ion in a neutral buffer gas is a function of gas properties such as pressure, temperature, and mass. It is also a function of parameters that affect momentum transfer, such as the structure and the interaction between the ion and gas [9]. The zero-field mobility can be approximated by the Mason-Schamp equation [5,10]:

$$K_I = \frac{v_d}{E} = \frac{3ze}{16N}\left(\frac{1}{m}+\frac{1}{M}\right)^{1/2}\left(\frac{2\pi}{k_bT}\right)^{1/2}\frac{1}{\overline{\Omega}_T^{1,1}}, \tag{2}$$

where m and M are the mass of the gas and the ion respectively, z is the number of charges, e is the elementary charge, N is buffer gas number density, k_b is Boltzmann constant, T is temperature, and $\overline{\Omega}_T^{1,1}$ is the average effective area of interaction at temperature T, which is known as collision cross-section (CCS). In the calculation of CCS, it is assumed that all orientations of the ion are equally probable, and the gas velocity is distributed according to a Maxwell-Boltzmann distribution. To calculate the CCS, a simplified equation which accounts for the momentum transfer from all directions by different gas velocities is given by [11,12]:

$$\overline{\Omega}_T^{1,1} = \frac{1}{8\pi^2}\int_0^{\pi} d\theta \int_0^{\pi} sin\varphi d\varphi \int_0^{\pi} d\gamma \frac{\pi}{8}\left(\frac{3}{K_bT}\right)^3 \int_0^{\infty} g^5 e^{-\frac{\mu g^2}{2K_bT}} dg \int_0^{\infty} 2b(1-cos\chi(\theta,\varphi,\gamma,g,b))db \tag{3}$$

In this equation, θ, φ, and γ are the orientation angles of the ion, g is the relative velocity, b is the impact parameter, $\mu = \left(\frac{1}{m}+\frac{1}{M}\right)^{-1}$ is the reduced mass, and χ is the deflection angle. The deflection angle depends upon relative velocity, impact parameter, orientation angles and ion-gas interaction parameters. The deflection angle can be calculated by [13,14]:

$$\chi(\theta,\varphi,\gamma,g,b) = \pi - 2b\int_{r_m}^{\infty}\frac{dr}{r^2\sqrt{1-\frac{b^2}{r^2}-\frac{\Phi(r)}{\frac{\mu g^2}{2}}}}. \tag{4}$$

$\Phi(r)$ is the ion-gas interaction potential being applied at distance r, where r varies from infinity to the distance of closest approach r_m. A comprehensive potential-interaction commonly used for polyatomic ions may be given by [11,15]:

$$\Phi(x,y,z) = 4\varepsilon\sum_{i=1}^{n}\left[\left(\frac{\sigma}{r_i}\right)^{12}-\left(\frac{\sigma}{r_i}\right)^{6}\right]-\frac{\alpha_p}{2}\left(\frac{ze}{n}\right)^2\left[\left(\sum_{i=1}^{n}\frac{x_i}{r_i^3}\right)^2+\left(\sum_{i=1}^{n}\frac{y_i}{r_i^3}\right)^2+\left(\sum_{i=1}^{n}\frac{z_i}{r_i^3}\right)^2\right] \tag{5}$$

In equation (5), n is the total number of atoms in the ion and r_i is the distance between the i^{th} atom and the gas molecule. The first term on the right-hand side corresponds to the 6–12 Lennard-Jones (L-J) potential acting between the i^{th} atom and the gas molecule where ε is the well depth and σ is the zero-potential crossing. The second term calculates the interaction due to the ion-induced dipole moment on the gas where α_p is the polarizability of the background gas. Given the geometrical complexity of the molecule, the calculation of eqs. (2)–(5) are almost exclusively done numerically. When an optimized geometrical structure is used and the correct numerical method is applied, it is customary to yield mobilities and CCS within 4% of the experimental counterpart [16–25]. It is perhaps necessary at this point to state that other potentials may be used or added, such as substituting the repulsion exponent for Buckingham potentials or for example adding ion-quadrupole potentials for N_2. Since the mobility depends on pressure and temperature, it is customary to provide a reduced mobility $\left(K_0 = K\frac{P}{760}\frac{273}{T}\right)$ at standard pressure and temperature [26–35].

Despite the success of the Mason-Schamp equation, its inability to be employed at higher fields precludes its use to determine mobilities for many instruments. Overall, eq. (2) should not be employed when the field over gas concentration, E/N, is of 10 Td or higher, although non-linear effects have been observed at much lower Td. Under weak fields, additional terms can be incorporated into eq. (2) to provide higher order approximations. For example the third order approximation to the mobility may be given by Ref. [36]:

$$K_{III} = K_I\left[\alpha_0 + \alpha_1\left(\frac{E}{N}\right)^2 + \alpha_2\left(\frac{E}{N}\right)^4 + \dots\right], \tag{6}$$

where the α_i values are functions of different collision cross section integrals [5]. Eq. (6) shows that only even powers of E/N are required. The reason why this expansion is only considered under weak fields revolves around the fact that the power series easily diverges due to unbounded nature of the $(E/N)^{2n}$ terms as the field is increased, requiring too many terms to reach medium to high field and eventually diverging.

A second possibility, and the one employed in this work, revolves around the use of the two-temperature theory [37,38]. The two-temperature theory, as its name suggests, requires the temperature of the ion, T_b, to be different from the gas temperature, T, to accommodate the energy derived from the electric field and the increasingly stronger collisions with the gas molecules. While the ion temperature is not known a priori, it is customary to use Wannier's formula as an estimate. With it, the ion temperature may be given by [39]:

$$\frac{3}{2}k_bT_b = \frac{3}{2}k_bT + \frac{1}{2}Mv_d^2 + \frac{1}{2}mv_d^2\,, \tag{7}$$

where the second and third terms on the right-hand side stand for the field and collisional energies (randomization of the field energy) respectively. Using this new temperature for the ion velocity distribution leads to the two-temperature expression for the mobility. The result is rather similar to expression (2) with the difference that an effective temperature T_{eff}, is used instead of temperature T:

$$K_{2TX} = \frac{3}{16}\frac{ze}{N}\left(\frac{2\pi}{\mu k_b T_{eff}}\right)^{\frac{1}{2}}\frac{(1+\alpha^*)}{\overline{\Omega}^{1,1}_{T_{eff}}} \tag{8}$$

$$\frac{3}{2}k_bT_{eff} = \frac{3}{2}k_bT + \frac{1}{2}mv_d^2(1+\beta^*) \tag{9}$$

Here X stands for the approximation number, and α^* and β^* stand for complex correction expressions that depend on the effective temperature, the mass ratio M/m, and the field to concentration ratio E/N ($\alpha^* = \beta^* = 0$ for the first-order approximation to the two-temperature theory). The α^* and β^* expressions were first calculated by Viehland et al. up to the 4th approximation [38]. $\overline{\Omega}^{1,1}_{T_{eff}}$ represents that the CCS must be now calculated at the effective temperature. Even for the first approximation, the simple change from T to T_{eff} allows for eq. (8) to be valid for the whole range of E/N. While there is an expectancy that higher approximations will yield overall higher accuracies, we really do not know the exact solution except for some specific cases (Lorentz model for electrons $\frac{M}{m} \ll 1$) [37]. For this reason, it is interesting to see how the different approximations behave as a function of the mass ratios M/m which is visualized in Fig. 1 A-D [37,38]. The y-axis in these set of figures represent the drift velocity deviations of higher approximations

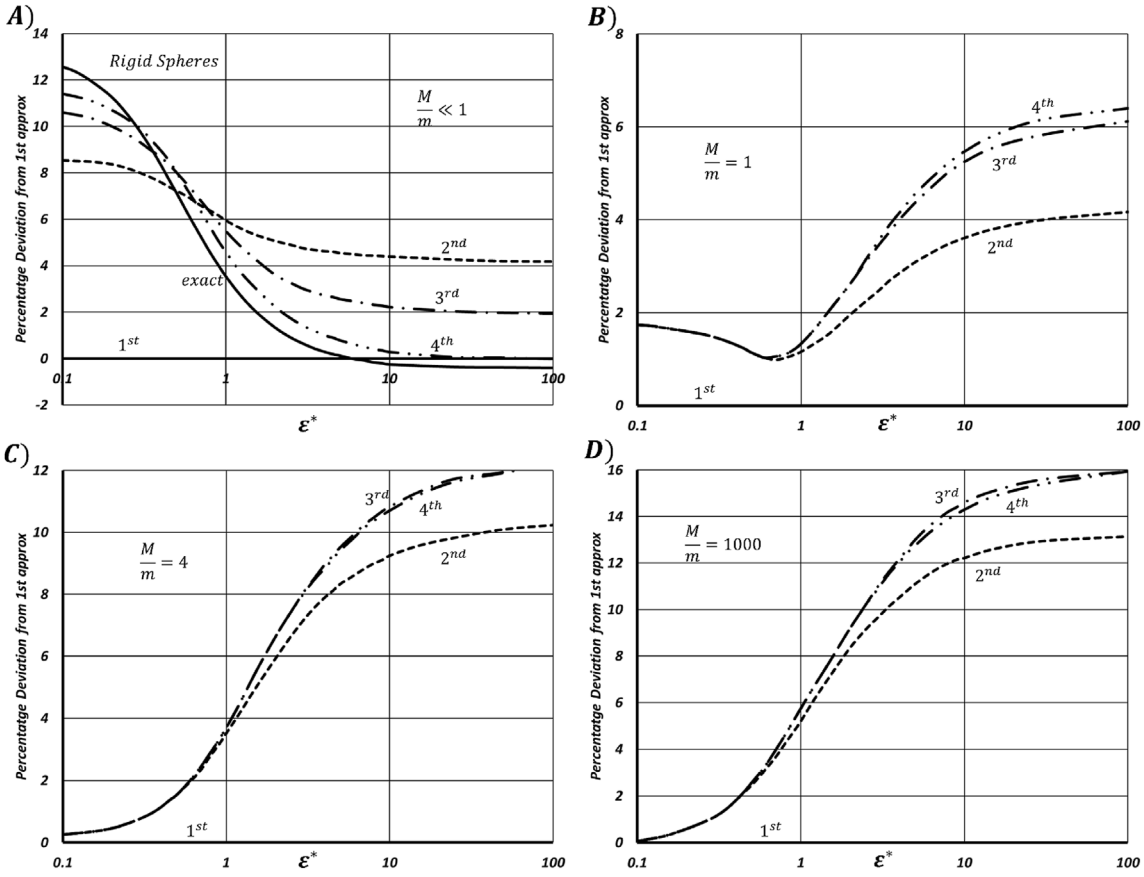

Fig. 1. Percentage of drift velocity deviation from the first order approximation to higher order approximations as a function of the dimensionless ε^* for different mass ratios a)$M/m \ll 1$, b)$M/m = 1$, c)$M/m = 4$, d)$M/m = 1000$. The y-axis is given by % *deviation* $= \frac{v_{dX} - v_{d1}}{v_{d1}}$, being X the approximation, while the x-axis is given by $\varepsilon^* = \left(\frac{3\pi^{1/2}}{16k_bT}\right)\left(\frac{m+M}{M}\right)^{1/2}\left(\frac{ze}{\Omega_s}\right)\left(\frac{E}{N}\right)$, where Ω_s corresponds to a CCS assuming gas and ion are rigid spheres. Figure is extracted from Ref. [37].

with respect to the first approximation which is given as a function of ε^*, a dimensionless number proportional to E/N. There are a couple of notable general points to make in Fig. 1. The first is that higher order approximations seem to provide diminishing returns. In particular, for large ions (B-D), given the difference between approximations 2–4, the fourth approximation seems to be the most accurate through the whole range of E/N, and can be expected to be quite close to the exact solution. The second is that the first approximation seems to have a small error of 0 – 10% for most reasonable scenarios ($\varepsilon^* = 0 - 10$), with the smallest errors happening at the smallest fields for larger ions. Hence mobility calculations at any field should be possible using existing numerical calculators.

A concern that arises when dealing with the two-temperature approximation is that it was developed for atomic ions and gases, and as such, does not consider inelastic collisions. Inelastic collisions are expected to be considerable at high fields and care should be taken to consider them when necessary. However, as will be shown here, inelastic collisions are much less important for light monoatomic gases such as Helium and its effects can be mostly circumvented.

The purpose of this work is therefore to test whether existing numerical tools are capable of calculating ion mobility as a function of E/N for a series of small ions in light gases by using the effective temperature as the calculation temperature. While the theory exists, it has not been implemented to calculate mobility in polyatomic ions due to the fact that inelastic collisions could play a role. As such it is attempted here for the first time where it is shown that the effect is mostly negligible in helium and small gases, with an emphasis on the need to verify this point experimentally. The calculation is done first for the two-temperature first order approximation and subsequently for the fourth order approximation, as there is the expectancy that errors can be substantial at high fields for the first approximation as can be extracted from Fig. 1. This is accomplished while optimizing the L-J potentials for the whole electric field range. When using the fourth approximation, the result is expected to be very close to the experimental result, with the only difference being possible effects from higher order interaction potentials and from anisotropic inelastic collisions. This brings up the possibility of being able to predict mobility at high fields and to design experiments with the most favorable separation. Finally, we provide a suitable explanation of the hump effect that can be observed for many of the ions studied. This is done by understanding the effect that potential interactions have on mobility.

2. Methodology

An important issue that the general two-temperature theory does not address is the appearance of inelastic collisions in polyatomic systems at low and high fields [40]. The Wang Chang-Uhlenbeck-de Boer extension to the Boltzmann equation can deal with internal degrees of freedom, whose effect may be studied by assuming a single internal temperature T_i. The Wannier formula may then be modified to account for such effects [41]:

$$\frac{3}{2}k_b T_{eff}^{inel}\left(1+\frac{m}{M}\xi\right)=\frac{3}{2}k_b T_{eff}^{el}=\frac{3}{2}k_b T+\frac{1}{2}m v_{d_{inel}}^2 \tag{10}$$

where ξ is a dimensionless ratio that characterizes the fractional energy loss and depends on field strength [40]. In eq. (10), $v_{d_{inel}}$ is used to indicate that in a numerical calculation, internal degrees of freedom would be considered, and inelastic effects would be present. This drift velocity $v_{d_{inel}}$ is in general different from its monoatomic counterpart, which may be referred to as $v_{d_{el}}$. However, it

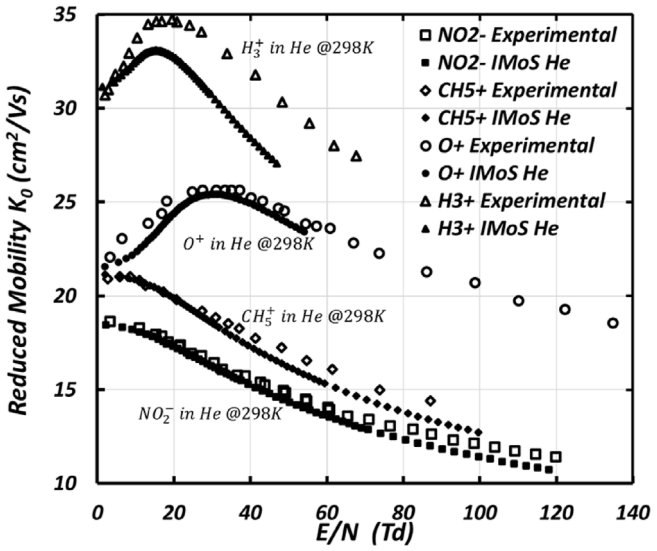

Fig. 2. Reduced mobility as a function of E/N in He gas for 4 different ions. Open symbols correspond to experimental results and closed symbols to numerical calculations performed with L-J parameters given in Ref. [42]. Figure extracted from Ref. [37].

can be shown that $T_i = T_{eff}$ when using atomic gases [40], in which case, the only possible difference between drift velocities comes from the excess in energy transfer to the gas upon collision. Under specular and isotropic conditions (all directions are equally probable), such as those predominantly occurring in He gas, it can be shown that this excess averages to zero when calculating the CCS and thus, $v_{d_{inel}} = v_{d_{el}}$, leaving the inelastic effects to ξ. However, calculating the effect of ξ would require at this point the knowledge of mobility as a function of temperature, which is not readily available. Given that the effect of ξ for monoatomic gases would only result in a scaling factor of the effective temperature, that the agreement must be exact at low fields ($\xi \to 0$), and that $m\xi/M$ should become smaller as the mass of the ion increases, the expectancy is that, for He, the effect of ξ will be minimal and may be circumvented by using instead an "elastic" effective temperature T_{eff}^{el} as the effective temperature to consider when comparing experiments and calculations, assuming a possible small error for polyatomic ions at moderate to high fields [40].

It must be noted that this method will not be valid for molecular and/or heavier gases or under strong potential interactions. This does not mean that the study cannot be equally performed, quite the contrary, but that it may be left to when sufficient data on molecular gases is available and the theory below is well established.

Existing numerical calculators such as IMoS make use of eqs. (2)–(5) or equivalent expressions to calculate the zero-field mobility and CCS as a function of the temperature [43]. One can take advantage of the fact that the first approximation to the two-temperature theory results in the same expression as eq. (2) but where an effective temperature T_{eff} is employed to account for the effect of the field. The idea is then that the temperature of the gas is assumed fixed (e.g., $T = 300K$) while the effective temperature becomes the temperature input in the program. Assuming $T_{eff} = T_{eff}^{el}$ to circumvent the appearance of ξ, the effective temperature may be converted to E/N, through the use of eqs. (1) and (9):

$$\frac{E}{N} = \frac{1}{K_I N}\left(\frac{3k_b\left(T_{eff} - T\right)}{m}\right)^{\frac{1}{2}}, \tag{11}$$

where $K_I = K_{eff_I} N_{eff}/N$ is a correction to the mobility obtained by IMoS, K_{eff_I}, that assumes the concentration N_{eff} is calculated at T_{eff} instead of T. Finally, the mobility can be written in terms of reduced mobility as: $K_0 = \frac{p}{101325}\frac{273.15}{T}K_I$. The validity of the results using L-J TM in helium using default L-J parameters have been preliminary tested and compared to experiments yielding very promising results [37]. The results are repeated here for convenience in Fig. 2. Note that the numerical calculations are capable of reproducing the variation of mobility quite satisfactorily despite the very different behaviors of the ions, increasing or decreasing their mobility with the electric field. In the discussion section, an explanation of the reason for the different behaviors is provided. Given these results, one can ponder the possibility of optimizing the L-J potentials to allow for a greater accuracy in the full E/N range using monoatomic ions when possible to avoid inelasticity issues. This can be done using the first order approximation or correcting the results to the 4th order approximation.

2.1. Density functional theory (DFT) calculation of small ions

In order to calculate the CCS and mobility of ions, an optimized geometrical model of the all-atom structure is required. An initial geometry of the molecule is created in Avogadro [44] using Molecular Mechanics (MM2) calculation. Frequency and geometry optimized structures using B3LYP [45–48] functional, and 6-31G(d,p) [49] Pople basis were then obtained for a series of small ions including H_3^+, O^+, CH_5^+, NO_2^-, O_2^+, NO^+, CO_2^+, N_2OH^+, NH_3^+, NH_4^+, H_2O^+, O_2H^+, COH^+. Larger ions were also calculated to test the validity of the new optimized parameters at zero field. These include Thymine, 1,2,4,5-Benzenetetramine, Guanine, Amantadine, 4-Aminosalicylic acid, 5-Aminosalicylic acid, Nicotine, Carbazole, Epinephrine, Paraquat, 9(10H)-Acridanone, 9,10-Dihydro-9,9-dimethylacridine, Carbamazepine, Mefenamic acid, Flufenamic acid, Colchicine, Saccharin, Methyl-2,6-dichloronicotinate, 5,7-Dichloro-8-quinolinol, Leflunomide, Methylene blue, 3,5-Dibromoant-hranilic acid, 3,4,5-Tribromopy-ridine. Finally Structures for Triphenylene, N-ethylaniline, Dexamethasone, Acetaminophen, Betamethasone, Anthracene, Choline, Phenanthrene, Acetylcholine, C_{70}, C_{60}, Naphtalene, Paracetamol, Pyrene, TtEA, TMA were taken from the software package IMoS [42]. The optimized structures have been included in the supplementary information.

2.2. Experimental mobility

Experimental reduced mobilities as a function of E/N in Helium gas were obtained Ellis et al. [32] (H_2O^+) and Ellis et al. [33] (O^+, O_2^+, H_3^+, N_2OH, NH_3^+, NH_4^+, CH_5^+, CO_2^+, COH^+, O_2H^+, NO_2^-, NO^+). The results from Ellis were a tabulation from the data from Lindinger and Albritton [50,51]. Despite these works being some of the most comprehensive empirical results as a function of the number of Townsend, it must be noted here that an error of 7% on the experimental results is mentioned. The value of mobility C_{60}^+ as a function of temperature was taken from Mesleh et al. [11] Experimental CCS at zero field given in Table S.2 were obtained from Campuzano et al. [18] for Triphenylene, N-ethylaniline, Dexamethasone, Acetaminophen, Betamethasone, Anthracene, Choline, Phenanthrene, Acetylcholine, C_{70}, C_{60}, Naphtalene, Paracetamol, Pyrene, TtEA, TMA and from Lee et al. [52] for over 20 other compounds including Thymine, Guanine, Amantadine, Nicotine, Carbazole, Epinephrine, Paraquat, Carbamazepine, Mefenamic acid, Flufenamic acid, Colchicine, Saccharin, Leflunomide and Methylene blue.

2.3. Optimization of L-J potentials using the first order approximation

The optimization of L-J potentials over the whole Townsend range can be done in a similar fashion to what has been attempted previously [9]. A tutorial to calculate mobility and optimize L-J parameters for a non-vanishing field is provided in the IMoS manual [42]. Briefly, a quadratic multidimensional error function $\mathscr{F}$ is created that may be used to minimize the difference between experimental and numerical mobilities as a function of the zero-crossing and well depth parameters of the atoms being optimized:

$$F(\varepsilon_1,\sigma_1,\varepsilon_2,\sigma_2,\ldots,\varepsilon_k,\sigma_k) = \sum_{i=1}^{i=n}\sum_{j=1}^{j=e}\left(1 - \frac{K_{0_{i,jCalc}}(\varepsilon_1,\sigma_1,\varepsilon_2,\sigma_2,\ldots,\varepsilon_k,\sigma_k)}{K_{0_{i,jExp}}}\right)^2. \tag{12}$$

Here, $K_{0_{i,jCalc}}$ and $K_{0_{i,jExp}}$ are the simulated and experimental reduced mobilities of the i^{th} ion at the $j^{th}E/N$ field value, k is the total number of elements (i.e., C, H, O, N) for which the L-J parameters are being optimized, n is the number of ions, and e is the number of different E/N (or T_{eff}) values employed. In this minimization problem, for the solution to be mathematically unambiguous, there must be at least two distinct experimental data points per element (one for each L-J parameter). This may be in the form of mobilities from two different ions but also from the same ion at different E/N, so the data is generally overdetermined. While an optimization method may be employed to solve eq. (12) (e.g., conjugate gradient), it has been shown that the optimization of the

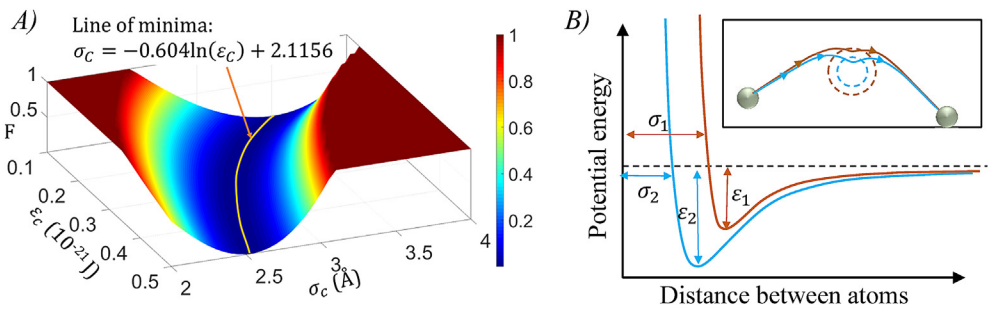

Fig. 3. A) Mapped surface of function $\mathscr{F}$ as a function of ε_C and σ_C. B) Illustrative representation for how two different L-J parameter pairs yield the same deflection angle.

$\varepsilon-\sigma$ pair in this way for a particular element is not necessarily unique. Instead, a *ceteris paribus* approach with a surface mapping procedure has been employed to observe whether a single minimum exists or rather "a line of minima" as is shown in Fig. 3 A). In other words, an iterative procedure is pursued where only one $\varepsilon-\sigma$ pair is minimized at a time while keeping the rest constant. One particular issue that arises when using eq. (12) is that once an effective temperature T_{eff} is chosen to calculate the mobility, the E/N value is unknown a priori, as it depends on the resulting mobility as shown in eq. (11). After E/N has been calculated, the discrete tabulated experimental mobility, $K_{0_{i,jExp}}$, has to be interpolated to the correct value so that the same E/N is employed for both simulation and experiment. A second requirement of this optimization is that the zero-field CCS calculations still maintain a similar level of accuracy as before. For this reason, a series of "control" ions are set as a constraint at low fields to keep the L-J parameters from diverging too much from their expected values.

It is noteworthy to mention that the experimental mobility K_{exp} could have been used instead of K_I in eq. (11) to transform experimental E/N into T_{eff} and compared with numerical results. This would avoid the issue of E/N not being known initially. However, given experimental errors (~7%), this option was not pursued.

2.4. Optimization of L-J potentials using the fourth order approximation

Using just the first approximation of the two-temperature theory to optimize the L-J potentials deals with the unfortunate consequence that any errors from the approximation must be embedded into the L-J potentials. This may question the overall universal validity of the results. While obtaining higher order approximations is in principle not possible with existing mobility calculators [42,53,54], given that the deviation from the first order approximation is known as provided in Fig. 1, one can still attempt to adjust the results by providing a correction to the mobility using tabulated data. The idea is therefore to initially calculate the two-temperature first order approximation to the mobility using IMoS at different effective temperatures. The effective temperature is then transformed into E/N using eq. (11), with the added difficulty that E/N has a dependency on the mobility so this transformation is different for each L-J parameter pair employed. The dimensionless field ε^* is subsequently obtained where Ω_s is calculated using the Projection Approximation (PA) on the DFT structures, followed by a correction mobility shift to the fourth order approximation interpolating the errors from Fig. 1 depending on the M/m ratio. Finally, this is compared to the experimental results. The end result is therefore equivalent to a mobility calculation using the fourth approximation, which can therefore be compared to the experimental values. Assuming the fourth approximation is exact, the L-J potentials optimized in this way should be much more universal and are expected to be more accurate for the whole E/N range.

The optimization of these potentials comes with the unwanted burden that there exist too many parametrizations of the L-J parameters that ultimately confuse the user. For this reason, this is meant to be more of a pedagogical exercise into the ability to calculate mobility at higher fields rather than an attempt at modifying yet again the L-J parameters.

Table 1
Optimized L-J parameters for the first and the fourth order approximation of the mobility equation.

L-J Atom pair	Using L-J given in ref [18]		1st order L-J parameters		4th order L-J parameters	
	$\varepsilon(10^{-21}\text{J})$	$\sigma(\text{Å})$	$\varepsilon(10^{-21}\text{J})$	$\sigma(\text{Å})$	$\varepsilon(10^{-21}\text{J})$	$\sigma(\text{Å})$
C−He	0.213	3.013	0.233	2.998	0.233	2.998
O−He	0.172	2.434	0.253	2.390	0.210	2.505
H−He	0.099	2.261	0.365	1.847	0.112	2.245
N−He	0.236	3.347	0.370	2.500	0.171	2.675

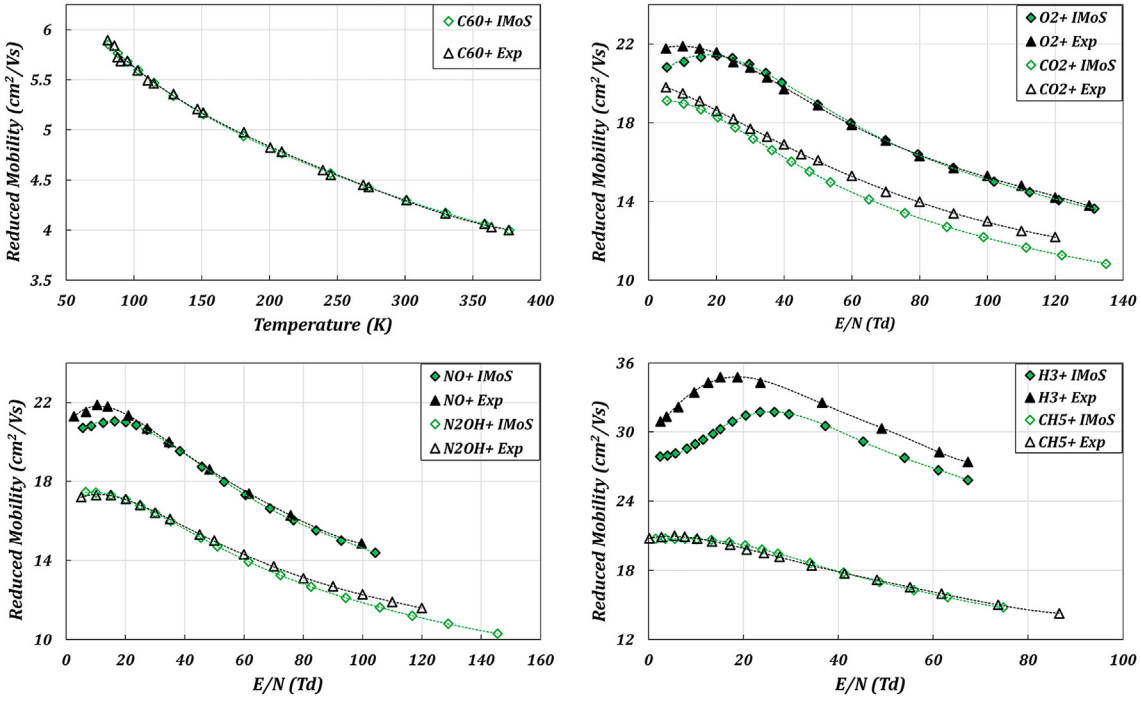

Fig. 4. Top left. Reduced mobility as a function of gas temperature for C_{60}^+ in He conditions which is used as a control for the rest of the ions [11]. Rest. Comparison between experimental and simulated reduced mobility as a function of E/N with L-J parameters optimized using the first approximation to mobility assuming a gas temperature of 300 K for $O_2^+, CO_2^+ (topright), NO^+$, $N_2OH^+ (bottomleft)$, H_3^+ and $CH_5^+ (bottomright)$

3. Results and discussion

To test the capability of using IMoS as a function of temperature, experimental results from Mesleh et al. were employed using C_{60}^+ and the standard L-J parameters given there for C–He pair [9,11]. The results are shown in Fig. 4 (top left) where excellent agreement between experiments and simulation may be observed. These results will also serve as a control to make sure that modifications of the L-J parameters do not excessively affect the zero-field results.

3.1. Results using the first order approximation to the two-temperature theory

To optimize L-J parameters for the first order approximation for elements C, O, H and N, six analytes (C_{60}^+, CH_5^+, O_2^+, CO_2^+, NO^+ and N_2OH^+) were chosen. Carbon is re-optimized following the results of C_{60}^+ at different temperatures.

Oxygen is optimized using O_2^+ and CO_2^+, Nitrogen is optimized using NO^+ and N_2OH^+, and Hydrogen is optimized using CH_5^+. To give an example of how the optimization is pursued through surface mapping, the error function ($\mathscr{F}$) for Carbon and C_{60}^+ is plotted as a function of ε_C and σ_C in Fig. 3 A). The value of $\mathscr{F}$ has been clipped at a certain height to accent the valley for representation purposes. From Fig. 3 A), it is clear that there is a line of minima instead of a single or apparent minimum. There exists a mathematical relationship between ε_c and σ_c which allows an infinite pair of combinations and the coefficient of determination (R2) of the minima line $\sigma_C = -0.604\ln(\varepsilon_C) + 2.1156$ is greater than 0.99. Any ε_C-σ_C pair that complies with the line of the minima is a suitable candidate for the optimization. The reason for multiple possibilities is depicted in Fig. 3 B) where two different pairs may still reproduce the same deflection angle making either choice virtually indistinguishable from each other when only CCS are used for the optimization [9]. It was speculated that a clear minimum could be observed using mobility at different temperatures, however, this is clearly not the case, at least generally. Although the minimum value of the error function for carbon was made to be at $\sigma_C = 2.9975$ Å and $\varepsilon_C = 0.2325(10^{-21}J)$, it would be an overstatement to claim this pair as a clear optimum, since the value of the error function throughout the line of minima stays relatively constant. The choice was made trying to keep the parameter values (in particular the zero crossing) physically reasonable (i.e., having the zero-crossing value being close to the sum of the values of the Van der Waals (VdW) radii).

The mapped surfaces of $\mathscr{F}$ for Oxygen, Hydrogen, and Nitrogen are given in Fig. S1. All the different elements show a similar pattern of having a line of minima, but where in some instances, a more clearly defined minimum is apparent within the line of minima. The equation for the line of minima for Oxygen, Hydrogen, and Nitrogen are $\sigma_O = -0.254\ln(\varepsilon_O) + 2.0217$, $\sigma_H = -0.24\ln(\varepsilon_H) + 1.5822$, and $\sigma_N = -0.283\ln(\varepsilon_N) + 2.2058$ respectively. The optimized L-J parameters values for the two-temperature first approximation are given in Table 1. A comparison of the reduced mobility vs E/N (or temperature in the case of C_{60}^+) between experimental and simulated data using optimized L-J parameters is given in Fig. 4. The first thing to note is the remarkable agreement between numerical and experimental results for most of the ions studied, despite the large range of E/N and the very different behaviors in mobility. This is even the case for the "enfant terrible" CH_5^+ for which a trigonal bipyramid structure was employed [55]. For small values of E/N, ion mobilities tend to plateau or increase with increasing E/N. For those that increase, a maximum value is eventually reached after which the reduced mobility becomes a monotonically decreasing function as E/N increases, creating a hump-like structure. The location of the maximum, if it exists, varies from ion to ion and a physical explanation for the occurrence is given below.

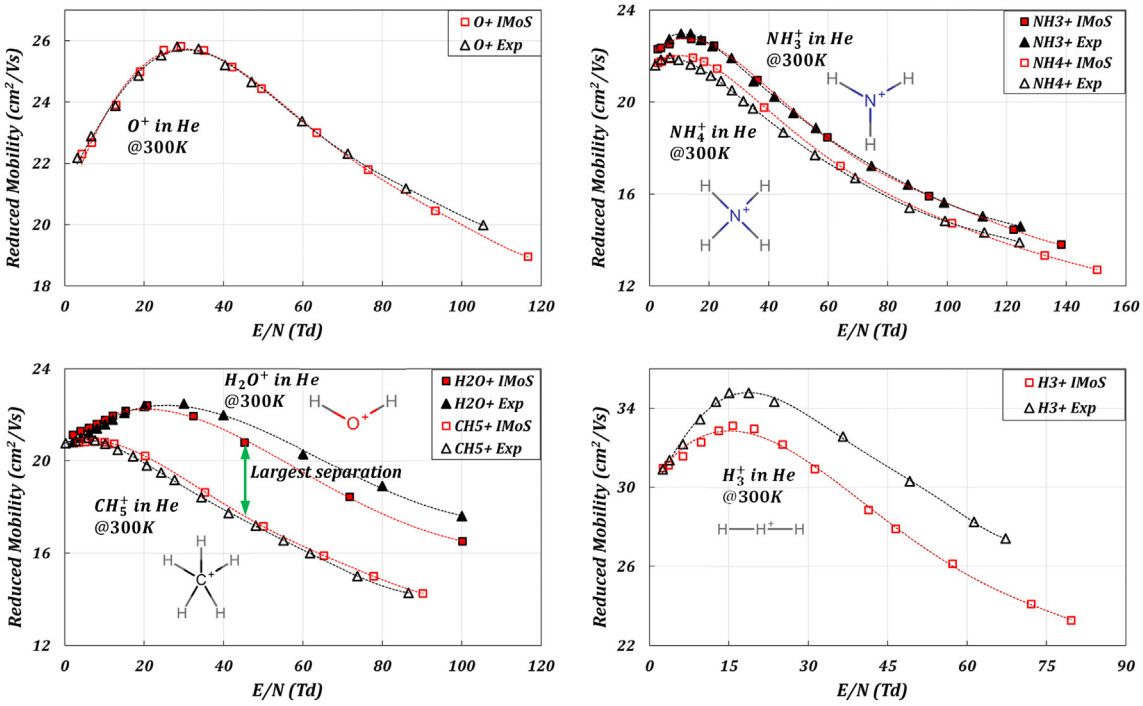

Fig. 5. Comparison between experimental and simulated reduced mobility as a function of E/N with L-J parameters optimized using the fourth approximation assuming a gas temperature of 300 K for O^+(*topleft*), NH_3^+, NH_4^+(*topright*), H_2O^+, CH_5^+ (*bottomleft*) and H_3^+ (*bottomright*).

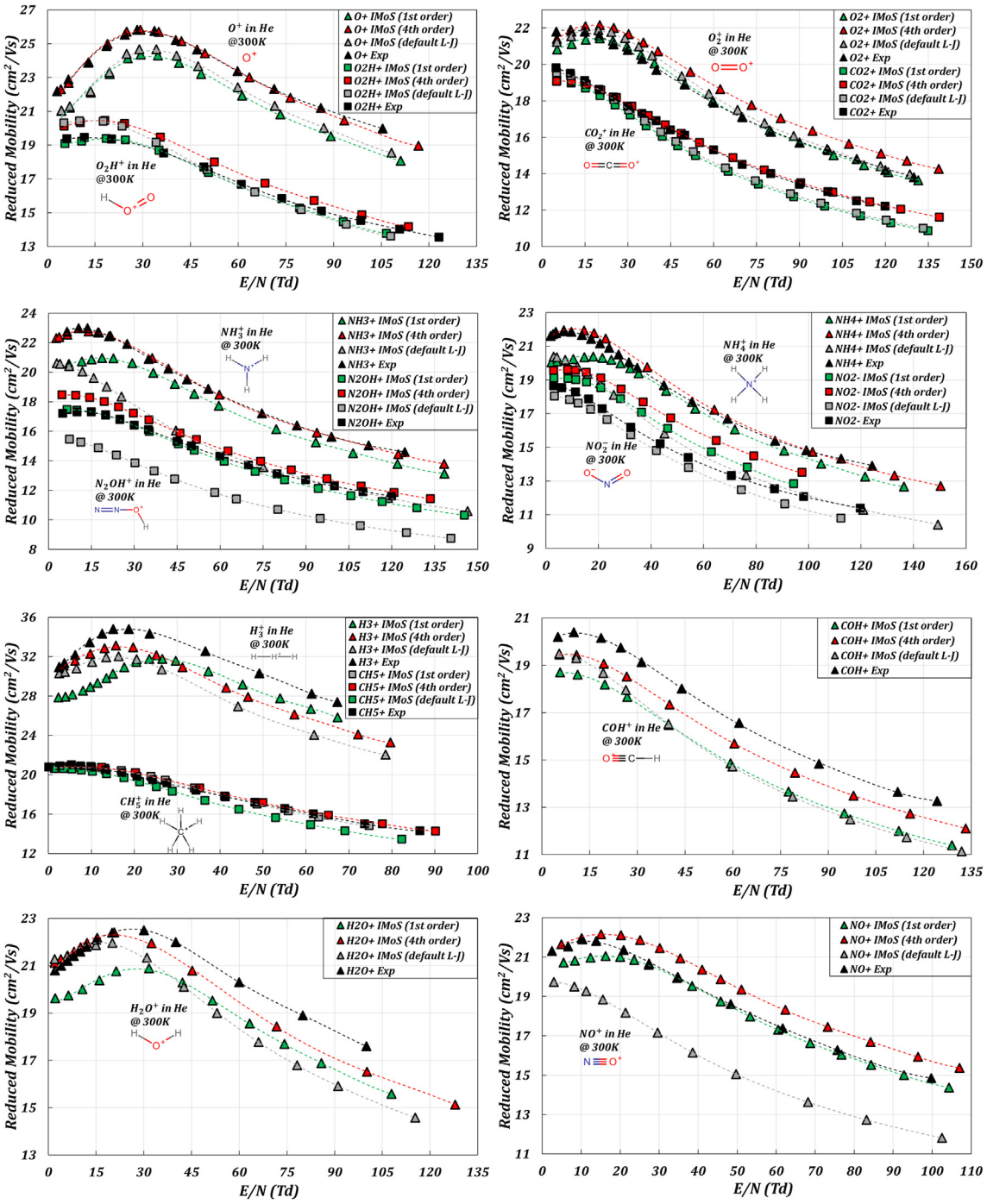

Fig. 6. Comparison of reduced mobility with respect to E/N between experimental results and the first and fourth approximation for ions from Figs. 4 and 5 and for other ions.

3.2. Results using the fourth order approximation to the two-temperature theory

Given that the L-J parameters of Carbon were optimized at different temperatures but assuming a zero-field regime, it is expected that the optimized Carbon parameters remain the same for the fourth as for the first order approximation. To optimize other atoms, one can follow the procedure from the method's section. In this case, O^+ was used to optimize Oxygen. Given that gas and ion are two atomic entities in this case, there are no inelastic collisions and therefore the kinetic theory results are expected to be exact. Nitrogen and Hydrogen were optimized using NH_3^+ and NH_4^+. Mapped surfaces of the error function $\mathscr{F}$ for the different iterations are plotted in Figs. S2 and S3. The optimized L-J parameter values of O, N and H are given in Table 1.

Comparison of the reduced mobility vs E/N between experimental and simulated data using optimized L-J parameters for the fourth approximation is given in Fig. 5. Once again, the numerical calculations follow the trends remarkably well; in particular for O^+, which is virtually exact as expected. In some of these ions, the hump that was observed previously is even more pronounced and the fact that the numerical results follow the trend so accurately

validates the method. This is the first time, to our knowledge, that calculations at high field and fourth order accuracy to the two-temperature theory have been performed for all-atom models consistently. Hence the method can be used to predict when the separation will be largest between two ions as visualized in the bottom left of Fig. 5, even though the ions might not be separable at zero field.

3.3. Results of optimization, comparison between approximations, and confirmation that CCS accuracy is maintained at zero-field

Given that different ions were used to optimize the first and fourth order approximations, it is necessary to validate if the new optimization parameters work for all ions. Fig. 6 shows the reduced mobility as a function of E/N for a compendium of ionic structures. Simulations results follow the correct behavior for all ions, even for those ions that differ somewhat from the experimental results. Table S1 provides the average error for each of the ions. This is obtained by calculating the difference between experimental and numerical calculations at the different E/N values over the full range where data is available. The results show that the optimized L-J parameters for the fourth approximation have an average error of 3.40% while those for the first approximation L-J parameters have an error of 4.26% (the error is 9.08% if the default L-J parameters were used to calculate mobility using the first order approximation). Given that the experimental results are expected to have errors of around 7%, one can indeed claim that the simulations using this simple procedure can calculate mobilities as a function of the field for small ions in He gas. This could easily be extended to other ions and gases if more accurate data were available, including the possibility of incorporating inelastic effects and deviation of internal temperatures T_i. It could also be extended to ions that are not rigid, by using an appropriate set of structures that represent the ensemble at that particular temperature.

One can further discuss the results showcased in Fig. 6. First, it seems quite clear that the results benefit from the optimization of the L-J parameters at all fields. The first approximation seems to deviate from experiments at low fields more than the fourth approximation (e.g., NH_3^+, NH_4^+, NO^+, …). This can be attributed to the fact that the optimization corrects for the errors committed by the first approximation at high fields (which are expected to be between 5 and 15%), resulting in less accurate results at low fields. The 4th approximation does not have this effect. However, while the fourth approximation has errors below 2% for most ions along the whole field range, it does not fare well for some of the ions (e.g., NO_2^-). This effect is somewhat harder to understand and is attributed to two main effects, the existing experimental error (7%) and the fact that the ion in question was not used for the optimization of the L-J parameters.

Given the points addressed above, it would be beneficial to make sure that the optimized parameters in Table 1 still provide accurate values of CCS at zero-field. As such, Table S.2 shows a comparison between experiment and simulation at 300K for both first and fourth order approximations for a large set of ions. The estimated CCS values using the optimized L-J parameters of the first order approximation are consistently lower than the experimental values except for C_{60} and C_{70}. Given that C_{60} was used in the optimization, it is reasonable to think that an overestimation of the carbon element may lead to an underestimation of the other parameters leading to the issue observed. For example, using the overestimated L-J parameters of Carbon in CH_5^+ could result in the underestimation of the He-Hydrogen L-J pair. Still, the error is approximately 3% on average for the first approximation. When using the fourth approximation, the overall results are much more satisfactory with the error averaging around 1.5% (see Table S.2), even when C—He L-J pair is still slightly overestimated. Moreover, when DFT structures are correctly obtained, the CCS calculations should give reasonable results even when non-optimized elements (NOE) are present as shown in Table S.3.

3.4. Description of the evolution of mobility as a function of the field (explanation of the hump)

As has been previously reported, the reduced mobility as a function of the field can either increase (A-type), decrease (C-type) or increase and then decrease (B-type) for a specific range of E/N[56]. Ions may follow any of the three types, although it seems that most of them follow the B-type or C-type if a sufficient E/N range is accommodated. As shown in Fig. 7, for the range of 0—30 Td, O^+ behaves mostly as an A-type, H_3^+ behaves as a B-type and CO_2^+ behaves mostly as a C-type. If a different range is chosen, i.e., 0—60 Td both O^+ and H_3^+ are B-type. Moreover, mobility will eventually decrease for all ions with the field [2,5]. Finally, it is possible that CO_2^+ could also behave as a B-type if the ambient temperature would be lowered. How can one make this assumption? It seems that the specific mobility behavior arises from a combination of two main effects: the “capture” effect caused by long-range interactions, which is maximized at low temperatures and/or fields, and the drag force effect originating from direct

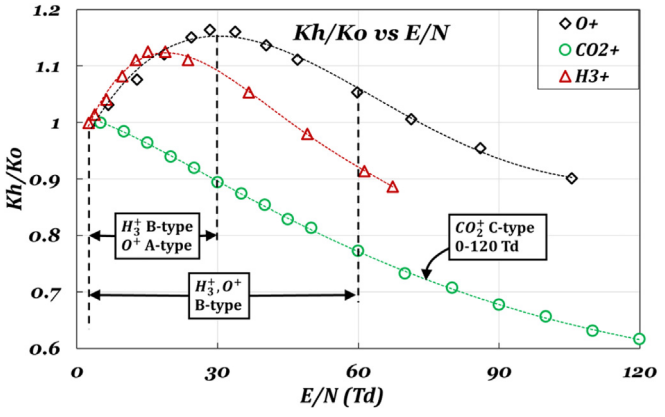

Fig. 7. Ratio of reduced mobility (Kh) to zero-field mobility (Ko) as a function of E/N for O^+, CO_2^+ and H_3^+.

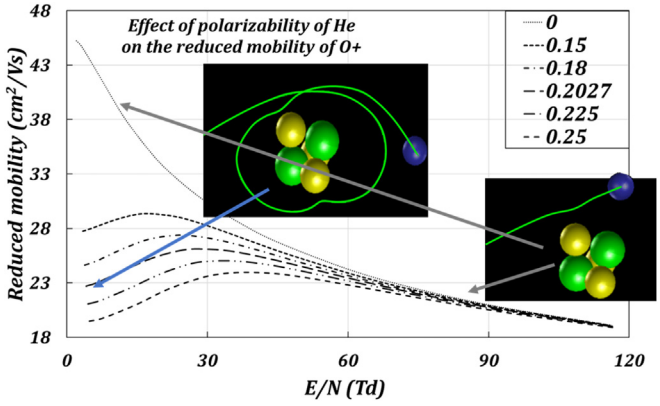

Fig. 8. Effect of Helium polarizability on reduced mobility as a function of E/N for the O^+ ion. This effect can be generalized for any ion as depicted on the insets representing the effect of strong (left) or weak polarizabilities (right).

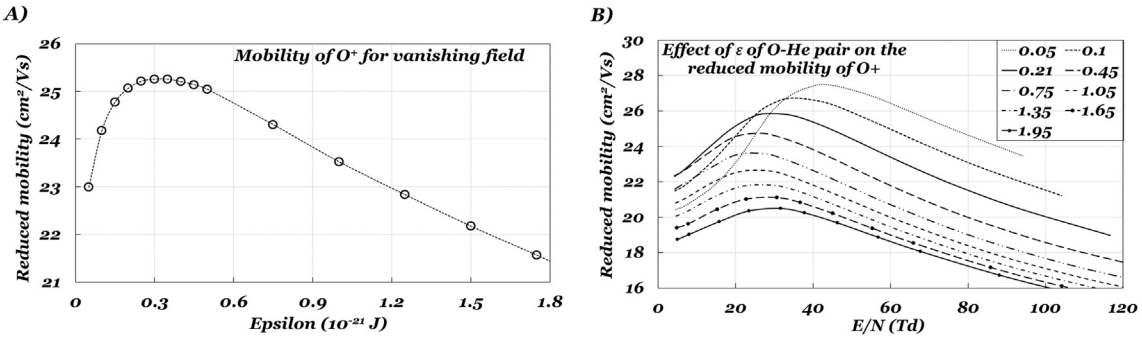

Fig. 9. The effect of the well-depth ε of the O–He pair on the mobility of the O^+ ion A) at zero field, B) as a function of E/N.

impingement momentum transfer which is maximized at high temperatures and/or fields.

At low fields (assuming constant gas concentration), the effect of long-range interactions may be quite significant reducing the mobility by means of a "capture" effect. This effect is enhanced for smaller ions, number of charges, and lower gas temperatures. A way to understand how long-range potentials affect the CCS is through the study of spherical ions. The potential interaction may be perceived as an effective increase of the ion's diameter that can be inferred [37]:

$$d_{eff}^2 = d^2\left[1 - \frac{\Phi(d)}{\frac{g^2\mu}{2}}\right] = d^2\left[1 - \frac{\Phi(d)}{\frac{3}{2}k_b T_{eff}}\right] \tag{13}$$

Here, d_{eff} is the enhanced collision diameter over the physical diameter d due to the interaction potential $\Phi(d) < 0$. The effect is softened by the relative kinetic energy, or equivalently, the effective temperature T_{eff} (and hence E/N). Therefore, increasing E/N reduces the effective diameter leading to an increase in mobility which produces the initial climb seen in some figures. This initial climb might not be present at high temperatures or for sufficiently large ions as the potential interaction may be too weak. As the field increases, on the other hand, the momentum transfer from direct impingement is enhanced due to the increase in relative kinetic energy, which results in a decrease in mobility. Since the potential interaction effect disappears with increased E/N, the reduction in mobility from direct impingement will eventually become predominant and therefore all ions should, sooner or later, become C-type. The impingement effect is enhanced for larger ions and higher gas temperatures which indicates that larger ions, e.g., C_{60}^+, only behave as C-type in He unless the gas temperature is markedly reduced.

To demonstrate the two effects, one can study the outcome of modifying the polarizability of the gas on the mobility as a function of the field. This has been done for O^+ in Fig. 8. For such as a small ion, the effect of polarizability is quite pronounced even in Helium gas. At zero polarizability, the ion behaves predominantly as a type-C ion, and only a small curvature is observed at small E/N which is attributed to the VdW interaction. As the polarizability is increased, the curvature becomes much more pronounced and is quite significant when the polarizability reaches $\alpha_p = 0.2073$ Å^3. However, regardless of the value of polarizability, the impingement effect dominates after ~60 Td where all lines start to converge.

Despite the relatively lower effect, one should be careful not to discard the effect of the VdW interactions in these small ions. One way to validate these effects is through the variational study of the L-J parameters. Due to the way expression (5) is constructed, the effect of the well depth ε is convoluted, as modifying its value influences both attractive and repulsive interactions. For this reason, it is not straightforward whether the variation of ε increases or reduces the mobility, even at zero field. Fig. 9 shows the variation of the mobility as a function of ε. As observed in Fig. 9 A), the effect of increasing epsilon at zero field initially increases the mobility, as for very small values of ε, the attractive interaction has a dominant effect (this depends on the value of σ) that allows the gas to be captured in the vicinity of the ion, yielding deflection angles that are quite large (lowering mobility). Eventually, as ε is increased, the repulsive portion starts to become important, lessening the aforementioned effect until the mobility reaches a maximum. The repulsive portion continues to become more dominant with further increases in ε, further reducing the mobility. The effect of epsilon as a function of E/N can be observed in Fig. 9 B), where the highest mobility is reached for the smallest ε, which does not necessarily represent the smallest mobility at zero-field. The effect of the long-range potentials may be severely enhanced by reducing the gas temperature. This could lead to very large changes of mobility in small changes of field and the effect could be used to separate ions which have very small differences in mobility at zero-field. Given the drastic effect in mobility that may result from modifying the long-range potentials and from changing the gas temperature. An important point to bring to the discussion is that one has to question the polarization limit model as it somewhat refutes the importance of temperature. While a polarization limit constant $K_{pol} = 13.853/(\alpha\mu)^{1/2}$ maybe a useful approximation, its exact result must be questioned as it is only useful at zero field and zero temperature [57].

The least accurate results in the simulations presented correspond to the H_3^+ ion. While experimental errors (of up to ~7%) could explain this difference, given the results from the rest of the ions, a second explanation is sought. Apart from being the smallest ion with the highest mobility, H_3^+ differs from the rest of the ions in that it is lighter than the Helium gas itself. A possibility for the deviation observed could be that inelastic collisions with the gas could lead to a change in the mobility. However, adding positive values of ξ would result in a bigger difference between theory and experiment so this avenue was not pursued. In this case, it is likely that the momentum collision integral term difference between impingement and reemitted relative velocities, namely $\vec{g} - \vec{g}'$, is no longer specular nor isotropic and hence its value differs strongly from our assumptions herein. This leads to the discussion of inelastic collisions. The reasonable assumption to make is that one has to be careful to incorporate inelastic collisions whenever possible. However, insufficient data is available at this time to incorporate ξ and hence the choice of small ions in light gases. Since for calculations at zero fields and different temperatures, the value of ξ is

necessarily zero, it is expected that a combination of mobility results at different temperatures and at different fields will lead to the optimization of both L-J parameters and ξ values rather accurately. Moreover, as more data becomes available for heavier gases such as N_2, a more in-depth study of the parameter ξ with respect to degrees of freedom and temperatures may be sought, including the prediction of the effect of internal temperatures and collision integral effects.

4. Conclusions

This manuscript is an attempt at consistent ion mobility calculations as a function of the field using all-atom models in Helium gas. The calculations have been performed using the first and fourth approximation to the two-temperature theory. The following conclusions may be extracted:

- The two-temperature theory consists of assuming a different temperature, T_b, for the ion. For the first approximation, this results in an integral quadrature for mobility quite similar to the zero-field, but where an effective temperature T_{eff} may be employed to simulate the effects of non-vanishing fields as a function of the electric field over the concentration, E/N. This leads to the possibility of regular mobility calculators, such as IMoS, to calculate mobilities for any field.
- The numerical calculations using first approximation to the two-temperature theory may have between 1 and 10% error depending on the mass ratio M/m. While mobility calculators cannot generally calculate the fourth approximation, a correction can be effectively used to overcome this drawback.
- Given the vast amount of data for small ions, an optimization of the L-J parameters for the first and the fourth order approximations is attempted. The resulting numerical mobilities have average errors for the whole field range of 4.26% for the first order (vs. 9.08% for the error using default L-J parameters) and 3.40% for the fourth order approximation when compared to their experimental counterpart, which is expected to have around a 7% error. While the fourth order approximation usually provides greater accuracy, the difference is not extremely significant on average. These results suggests that the effects of the higher-order terms, along with other effects such as vibration, ion-quadrupole potential, and diffuse collision can be embedded into L-J parameters without significant loss of accuracy as has been done in the past. However, since higher-order terms to the two-temperature approximation depend on the mass ratio of ion to gas, one should be careful with the selection of appropriate L-J parameters for mobility calculations if a large range of E/N is to be studied.
- In general, a line of minima is observed in the optimization of L-J parameters. This behavior can be reasoned from the calculations only requiring a deflection angle, which can be recreated for several different L-J pairs.
- The effects of well-depth ε and polarizability α_p were studied together with the overall relative kinetic energy. The combined effect is responsible for the hump-like effect in the $K_0 - E/N$ curves. As the effect of long-range potentials decreases with increasing field (due to an increase in the relative kinetic energy), the mobility increases. Simultaneously, the stronger impingement from the gas molecules as the field increases, decreases the mobility. There is therefore a competition between the two effects that establishes the curve. If a lower gas temperature is used, the effect of the hump may be enhanced which could be employed to improve separation of species even further.
- While inelastic collisions may be important for heavier molecular gases, they can be mostly neglected for Helium under the E/N range studied and hence predictions of mobility can be made very accurately for all-atom models.
- Finally, the ability to predict mobilities at different fields and/or temperatures, allows for the possibility to infer where the maximum mobility separation occurs between two ions prior to running a separation experiment.

Funding source

This work is supported by the National Science Foundation Division of Chemistry under Grant No. 1904879 (Program officer Dr. Kelsey Cook).

CRediT authorship contribution statement

Viraj D. Gandhi: Software, Validation, Investigation, Formal analysis, Data curation, Writing – review & editing, Visualization. **Carlos Larriba-Andaluz:** Conceptualization, Methodology, Software, Investigation, Resources, Writing – original draft, Writing – review & editing, Supervision, Project administration, Funding acquisition.

Declaration of competing interest

The authors declare that they have no known competing financial interests or personal relationships that could have appeared to influence the work reported in this paper.

Appendix A. Supplementary data

Supplementary data to this article can be found online at https://doi.org/10.1016/j.aca.2021.339019.

References

[1] G.F. Verbeck, B.T. Ruotolo, K.J. Gillig, D.H. Russell, Resolution equations for high-field ion mobility, J. Am. Soc. Mass Spectrom. 15 (2004) 1320–1324.
[2] A.A. Shvartsburg, R.D. Smith, A. Wilks, A. Koehl, D. Ruiz-Alonso, B. Boyle, Differential Ion Mobility Spectrometry: nonlinear Ion Transport and Fundamentals of FAIMS, 2008.
[3] E.V. Krylov, S.L. Coy, E.G. Nazarov, Temperature effects in differential mobility spectrometry, Int. J. Mass Spectrom. 279 (2009) 119–125.
[4] E. Krylov, E. Nazarov, Electric field dependence of the ion mobility, Int. J. Mass Spectrom. 285 (2009) 149–156.
[5] E.A. Mason, E.W. McDaniel, Transport Properties of Ions in Gases, John Wiley & Sons., New York, 1988.
[6] G.A. Eiceman, Advances in ion mobility spectrometry: 1980–1990, Crit. Rev. Anal. Chem. 22 (1991) 471–490.
[7] R.H. St Louis, H.H. Hill Jr., G.A. Eiceman, Ion mobility spectrometry in analytical chemistry, Crit. Rev. Anal. Chem. 21 (1990) 321–355.
[8] V. Gabelica, E. Marklund, Fundamentals of ion mobility spectrometry, Curr. Opin. Chem. Biol. 42 (2018) 51–59.
[9] T. Wu, J. Derrick, M. Nahin, X. Chen, C. Larriba-Andaluz, Optimization of long range potential interaction parameters in ion mobility spectrometry, J. Chem. Phys. 148 (2018), 074102.
[10] J.O. Hirsehfelder, C.F. Curtiss, R.B. Bird, Molecular Theory of Gases and Liquids, New York, 1954.
[11] M. Mesleh, J. Hunter, A. Shvartsburg, G.C. Schatz, M. Jarrold, Structural information from ion mobility measurements: effects of the long-range potential, J. Phys. Chem. 100 (1996) 16082–16086.
[12] A.A. Shvartsburg, M.F. Jarrold, An exact hard-spheres scattering model for the mobilities of polyatomic ions, Chem. Phys. Lett. 261 (1996) 86–91.
[13] C.H. Kruger, W. Vincenti, Introduction to Physical Gas Dynamics, John Wlley & Sons, 1965.
[14] Z. Li, H. Wang, Drag force, diffusion coefficient, and electric mobility of small particles. I. Theory applicable to the free-molecule regime, Phys. Rev. E - Stat. Nonlinear Soft Matter Phys. 68 (2003), 061206.
[15] C. Larriba-Andaluz, F. Carbone, The size-mobility relationship of ions, aerosols, and other charged particle matter, J. Aerosol Sci. (2020) 105659.
[16] F. Furche, R. Ahlrichs, P. Weis, C. Jacob, S. Gilb, T. Bierweiler, M.M. Kappes, The

structures of small gold cluster anions as determined by a combination of ion mobility measurements and density functional calculations, J. Chem. Phys. 117 (2002) 6982–6990.
[17] S. Gilb, P. Weis, F. Furche, R. Ahlrichs, M.M. Kappes, Structures of small gold cluster cations (Aun+, n<14): ion mobility measurements versus density functional calculations, J. Chem. Phys. 116 (2002) 4094–4101.
[18] I. Campuzano, M.F. Bush, C.V. Robinson, C. Beaumont, K. Richardson, H. Kim, H.I. Kim, Structural characterization of drug-like compounds by ion mobility mass spectrometry: comparison of theoretical and experimentally derived nitrogen collision cross sections, Anal. Chem. 84 (2012) 1026–1033.
[19] N.L. Zakharova, C.L. Crawford, B.C. Hauck, J.K. Quinton, W.F. Seims, H.H. Hill Jr., A.E. Clark, An assessment of computational methods for obtaining structural information of moderately flexible biomolecules from ion mobility spectrometry, J. Am. Soc. Mass Spectrom. 23 (2012) 792–805.
[20] H. Ouyang, C. Larriba-Andaluz, D.R. Oberreit, C.J. Hogan Jr., The collision cross sections of iodide salt cluster ions in air via differential mobility analysis-mass spectrometry, J. Am. Soc. Mass Spectrom. 24 (2013) 1833–1847.
[21] C. Lapthorn, T.J. Dines, B.Z. Chowdhry, G.L. Perkins, F.S. Pullen, Can ion mobility mass spectrometry and density functional theory help elucidate protonation sites in 'small' molecules? Rapid Commun. Mass Spectrom. 27 (2013) 2399–2410.
[22] C. Lapthorn, F.S. Pullen, B.Z. Chowdhry, P. Wright, G.L. Perkins, Y. Heredia, How useful is molecular modelling in combination with ion mobility mass spectrometry for 'small molecule' ion mobility collision cross-sections? Analyst 140 (2015) 6814–6823.
[23] P. Benigni, J.D. DeBord, C.J. Thompson, P. Gardinali, F. Fernandez-Lima, Increasing polyaromatic hydrocarbon (PAH) molecular coverage during fossil oil analysis by combining gas chromatography and atmospheric-pressure laser ionization fourier transform ion cyclotron resonance mass spectrometry (FT-ICR MS), Energy Fuels 30 (2016) 196–203.
[24] J. Boschmans, S. Jacobs, J.P. Williams, M. Palmer, K. Richardson, K. Giles, C. Lapthorn, W.A. Herrebout, F. Lemiere, F. Sobott, Combining density functional theory (DFT) and collision cross-section (CCS) calculations to analyze the gas-phase behaviour of small molecules and their protonation site isomers, Analyst 141 (2016) 4044–4054.
[25] I. Czerwinska, J. Far, C. Kune, C. Larriba-Andaluz, L. Delaude, E. De Pauw, Structural analysis of ruthenium-arene complexes using ion mobility mass spectrometry, collision-induced dissociation, and DFT, Dalton Trans. 45 (2016) 6361–6370.
[26] Z. Karpas, Ion mobility spectrometry of aliphatic and aromatic amines, Anal. Chem. 61 (1989) 684–689.
[27] H. Revercomb, E.A. Mason, Theory of plasma chromatography/gaseous electrophoresis, Anal. Chem. 47 (1975) 970–983.
[28] E. Mason, H. O'hara, F. Smith, Mobilities of polyatomic ions in gases: core model, J. Phys. B Atom. Mol. Phys. 5 (1972) 169.
[29] D. Parent, M. Bowers, Temperature dependence of ion mobilities: experiment and theory, Chem. Phys. 60 (1981) 257–275.
[30] L. Viehland, D. Fahey, The mobilities of NO− 3, NO− 2, NO+, and Cl− in N2: a measure of inelastic energy loss, J. Chem. Phys. 78 (1983) 435–441.
[31] L.A. Viehland, S. Lin, Application of the three-temperature theory of gaseous ion transport, Chem. Phys. 43 (1979) 135–144.
[32] H. Ellis, E. McDaniel, D. Albritton, L. Viehland, S. Lin, E. Mason, Transport properties of gaseous ions over a wide energy range. Part II, Atomic Data Nucl. Data Tables 22 (1978) 179–217.
[33] H. Ellis, R. Pai, E. McDaniel, E. Mason, L. Viehland, Transport properties of gaseous ions over a wide energy range, Atomic Data Nucl. Data Tables 17 (1976) 177–210.
[34] H. Ellis, M. Thackston, E. McDaniel, E. Mason, Transport properties of gaseous ions over a wide energy range. Part III, Atomic Data Nucl. Data Tables 31 (1984) 113.
[35] M. Tabrizchi, Temperature corrections for ion mobility spectrometry, Appl. Spectrosc. 55 (2001) 1653–1659.
[36] H.J. Cooper, To what extent is FAIMS beneficial in the analysis of proteins? J. Am. Soc. Mass Spectrom. 27 (2016) 566–577.
[37] C. Larriba-Andaluz, J.S. Prell, Fundamentals of ion mobility in the free molecular regime. Interlacing the past, present and future of ion mobility calculations, Int. Rev. Phys. Chem. 39 (2020) 569–623.
[38] L.A. Viehland, E. Mason, Gaseous ion mobility and diffusion in electric fields of arbitrary strength, Ann. Phys. 110 (1978) 287–328.
[39] G.H. Wannier, Motion of gaseous ions in strong electric fields, The Bell Syst. Tech. J. 32 (1953) 170–254.
[40] E.A. Mason, E.W. McDaniel, Transport Properties of Ions in Gases, 1988.
[41] L. Viehland, S. Lin, E. Mason, Kinetic theory of drift-tube experiments with polyatomic species, Chem. Phys. 54 (1981) 341–364.
[42] J. Coots, V. Gandhi, T. Onakoya, X. Chen, C.L. Andaluz, A parallelized tool to calculate the electrical mobility of charged aerosol nanoparticles and ions in the gas phase, J. Aerosol Sci. (2020) 105570.
[43] C. Larriba, C.J. Hogan, Free molecular collision cross section calculation methods for nanoparticles and complex ions with energy accommodation, J. Comput. Phys. 251 (2013) 344–363.
[44] M.D. Hanwell, D.E. Curtis, D.C. Lonie, T. Vandermeersch, E. Zurek, G.R. Hutchison, Avogadro: an advanced semantic chemical editor, visualization, and analysis platform, J. Cheminf. 4 (2012) 17.
[45] P.J. Stephens, F.J. Devlin, C.F. Chabalowski, M.J. Frisch, Ab initio calculation of vibrational absorption and circular dichroism spectra using density functional force fields, J. Phys. Chem. 98 (1994) 11623–11627.
[46] A.D. Becke, Becke's three parameter hybrid method using the LYP correlation functional, J. Chem. Phys. 98 (1993) 5648–5652.
[47] C. Lee, W. Yang, R. Parr, Density-functional exchange-energy approximation with correct asymptotic behaviour, Phys. Rev. B 37 (1988) 785–789.
[48] S.H. Vosko, L. Wilk, M. Nusair, Accurate spin-dependent electron liquid correlation energies for local spin density calculations: a critical analysis, Can. J. Phys. 58 (1980) 1200–1211.
[49] J.D. Dill, J.A. Pople, Self-consistent molecular orbital methods. XV. Extended Gaussian-type basis sets for lithium, beryllium, and boron, J. Chem. Phys. 62 (1975) 2921–2923.
[50] I. Dotan, W. Lindinger, D.L. Albritton, Mobilities of various mass-identified positive and negative ions in helium and argon, J. Chem. Phys. 64 (1976) 4544–4547.
[51] W. Lindinger, D.L. Albritton, Mobilities of various mass-identified positive ions in helium and argon, J. Chem. Phys. 62 (1975) 3517–3522.
[52] J.W. Lee, K.L. Davidson, M.F. Bush, H.I. Kim, Collision cross sections and ion structures: development of a general calculation method via high-quality ion mobility measurements and theoretical modeling, Analyst 142 (2017) 4289–4298.
[53] S.A. Ewing, M.T. Donor, J.W. Wilson, J.S. Prell, Collidoscope, An improved tool for computing collisional cross-sections with the trajectory method, J. Am. Soc. Mass Spectrom. 28 (2017) 587–596.
[54] C.A. Myers, R.J. D'Esposito, D. Fabris, S.V. Ranganathan, A.A. Chen, CoSIMS: an optimized trajectory-based collision simulator for ion mobility spectrometry, J. Phys. Chem. B 123 (2019) 4347–4357.
[55] T. Oka, Taming CH5+, the “enfant terrible” of chemical structures, Science 347 (2015) 1313–1314.
[56] R.W. Purves, R. Guevremont, S. Day, C.W. Pipich, M.S. Matyjaszczyk, Mass spectrometric characterization of a high-field asymmetric waveform ion mobility spectrometer, Rev. Sci. Instrum. 69 (1998) 4094–4105.
[57] E.W. McDaniel, Collision Phenomena in Ionized Gases, 1964.